JOURNAL OF THERMOPHYSICS AND HEAT TRANSFER
Vol. 8, No. 1, Jan.–March 1994

Review of Chemical-Kinetic Problems of Future NASA Missions, II: Mars Entries

Chul Park, John T. Howe, and Richard L. Jaffe
NASA Ames Research Center, Moffett Field, California 94035
and
Graham V. Candler
North Carolina State University at Raleigh, Raleigh, North Carolina 27607

Nomenclature

a = constant in Millikan-White correlation formula, dimensionless, Eq. (3)
b = constant in Millikan-White correlation formula, dimensionless, Eq. (3)
C = reaction rate constant, $cm^3\ mol^{-1}\ s^{-1}$, Eq. (20)
k = Boltzmann constant (1.3806×10^{-16} erg/K)
k_f = forward reaction rate coefficient, $cm^3\ mole^{-1}\ s^{-1}$
M = unspecified third body
m = mass of one particle, grams
n = pre-exponential temperature power, Eq. (20)
n_t = total number density of a gas mixture, cm^{-3}

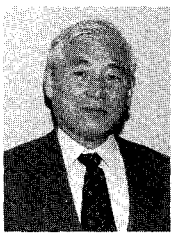

Chul Park is a Senior Staff Scientist at the NASA Ames Research Center in the Aerothermodynamics Branch. He joined Ames Research Center in 1964 as an NRC Research Associate. His pioneering works cover a wide range of topics on hypervelocity flight, from gas physics to application, on both theoretical and experimental aspects. He authored a book titled *Nonequilibrium Hypersonic Aerothermodynamics*. The author received a B.S. (1957) and an M.S. (1960) in Aeronautical Engineering from Seoul University and a Ph.D. (1964) in Aeronautics (hypersonics) from Imperial College of Science and Technology. The author is an Associate Fellow of AIAA.

John T. Howe, Chief Scientist at NASA Ames Research Center, received his B.S. from the University of Michigan in 1950 and his M.S. in 1956 and the degree of Engineer in 1958 from Stanford University, all in engineering mechanics. He teaches Hypervelocity Atmospheric Flight and Real Gas Phenomena at Stanford University. After a brief period with Stanford Research Institute, he joined the Ames Laboratory of NACA. During his 35 yr with NASA, he served as Senior Staff Scientist, Head of Aerothermodynamics, Assistant Chief for the Physics Branch, and Branch Chief for Fluid Dynamics. He is known for his pioneering research contributions to the aerothermodynamics of atmospheric entry, including radiative energy transfer, reactive gas flows, and innovative thermal protections systems. He was a member of the AIAA Thermophysics Technical Committee (1982–84) and an Associate Editor for the *Journal of Spacecraft and Rockets* (1982–84). He is a recipient of the AIAA Thermophysics Award (1986) and a Fellow of AIAA.

Richard L. Jaffe is a research scientist at the NASA Ames Research Center in the Computational Chemistry Branch. He joined Ames Research Center in 1976 and has been active in applying computational chemistry methods to problems in atmospheric chemistry, materials science, combustion chemistry, and aerothermodynamics. The author received a B.S. in Chemistry from the University of Rochester (1968) and a Ph.D. in Physical Chemistry from Yale University (1972). Prior to joining the Ames Research Center, he held a postdoctoral position at the University of Rochester and an NRC Associateship at NASA Ames.

Graham Candler is an assistant professor of Aerospace Engineering and Mechanics at the University of Minnesota. Previously, he was an assistant professor at North Carolina State University and an Aerospace Engineer at the NASA Ames Research Center. His research interests are the numerical simulation of nonequilibrium reacting flows, high temperature gas dynamics, and hypersonic aerodynamics. The author received a B.Eng. (1984) from McGill University and an M.S. (1985) and Ph.D. (1988) in Aeronautics and Astronautics from Stanford University. He is a member of the AIAA.

Presented in part as Paper 91-0464 at AIAA 29th Aerospace Sciences Meeting, Reno, NV, Jan. 7–10, 1991; received Nov. 12, 1992; revision received April 26, 1993; accepted for publication May 7, 1993.

p = pressure, Pa or atm
q_r = radiative heat flux at stagnation point, W/cm^2
R = nose radius, m
T = heavy particle translational-rotational temperature, K
T_a = geometric average temperature, $\sqrt{TT_v}$, K
T_d = characteristic temperature of reaction, K, Eq. (20)
T_v = vibrational-electron-electronic temperature, K
T_x = unspecified temperature (T, T_a, or T_v), K
U_s = shock velocity in a shock tube, km/s
V = flight velocity, km/s
θ = characteristic vibrational temperature, K
μ = equivalent molecular weight, g/mol
ρ = density, kg/m^3
σ_v = collision-limited vibrational cross section, Eq. (4), cm^2
σ_v' = collision-limited vibrational cross section at 50,000 K, Eq. (5), cm^2
τ = characteristic time, s or μs
τ_v = vibrational relaxation time, s or μs

Subscripts
s = postshock condition
1 = condition ahead of shock wave
2 = condition immediately behind shock wave
5 = condition in reflected-shock region
∞ = freestream

Introduction

THE escape velocity for the planet Mars is 5.0 km/s. Minimum-energy flight trajectories from Earth to Mars result in a Martian entry velocity of 5.8 km/s or slightly higher.[1] Such a flight trajectory requires a one-way trip time of nearly 1 yr. For a manned mission, such a long journey is undesirable. A faster trip is possible using a high-energy trajectory, but such fast trips result in a higher entry velocity. The compromise between the trip time and the entry velocity leads to a scenario requiring a one-way trip time of 5–8 months, and an entry velocity between 7–9 km/s.[1-3] The use of aerobraking technology can potentially allow significant reduction in the initial mass of the vehicle for this type of mission.

In the recent unmanned space missions, the chemical composition of the Martian atmosphere has been determined to be 95.7% CO_2, 2.7% N_2, and 1.6% Ar.[4] The shock layer flow for the Martian entry flight will contain C, CO, C_2, and CN, all of which are known to have mechanisms for strong radiation.[5] In the case of air, strong radiation is emitted from the nonequilibrium region behind a shock wave at flight velocities below about 10 km/s.[6] One would like to know whether the same is true in the Martian atmosphere, and if so, the size of the nonequilibrium region and the intensity of the resulting radiation.

No kinetic or radiation measurements have yet been made with the Martian gas mixture. However, a fair amount of theoretical and experimental investigations have been made for mixtures containing CO_2 or CO. For CO, the observed vibrational relaxation behavior behind a shock wave was found to be representable closely with the Millikan-White correlation formula at relatively low temperatures.[7] The vibrational relaxation behavior of CO_2 was also characterized using a similar correlation formula.[8] A considerable amount of experimental data exist on the dissociation of CO_2, CO, and CN, and on the exchange reactions containing these gases. They are reviewed in Refs. 9 and 10. More recent data will be discussed later. These existing experimental data are for temperatures up to about 15,000 K. The translational temperatures immediately behind the shock wave (prior to onset of vibrational excitation), corresponding to flight speeds of 6 and 9 km/s, are 25,000 and 59,000 K, respectively, for the Martian gas mixture, while the corresponding equilibrium temperatures are about 4800 and 7300 K. It has not been shown that the existing reaction rate coefficient set can be used for reliable predictions of thermochemical processes at such temperatures.

Theoretical studies of vibrational relaxation phenomena in CO_2 and CO have been made by Hindelang[11] and Hahne,[12] respectively. A complicated internal nonequilibrium process was described for CO_2 by Hindelang, while a relatively simple, Landau-Teller type relaxation was predicted for CO by Hahne. The combined chemical-fluid mechanical relaxation problem has been studied theoretically by Howe,[13,14] McKenzie,[15] Freeman and Oliver,[16] and Candler.[17] Howe estimated the reaction rate constants from kinetic theory, and concluded that the equilibration distances for CO_2 are fairly large under the typical conditions of Martian entry. McKenzie obtained his reaction rate coefficients both from estimates and from available experimental data. He did not calculate the equilibration distance, but instead calculated the radiation overshoot phenomenon in the nonequilibrium region. Freeman and Oliver predicted a fairly large chemical equilibration distance, and predicted that the radiative heating rate of a Martian entry vehicle may be increased by a large factor by chemical nonequilibrium phenomena. Candler predicted the relaxation distance in the Martian gas mixture to be considerably smaller than the value predicted by Howe. All theoretical calculations predicted that vibrational relaxation would reach equilibrium quickly in a predominantly CO_2 mixture.

Experimental investigations of the nonequilibrium radiation behavior in CO_2 or CO_2-N_2 mixture were made by Arnold et al.[18] Thomas and Menard,[19] Nealy and Haggard,[20,21] and Arnold and Nicholls.[22] In Ref. 20, Nealy and Haggard made measurements of the radiation from CO_2 in the vacuum-uv wavelength range, and applied the experimental data to predict the impact of nonequilibrium in the radiative heating of the Venusian entry probe. A modest increase (about 30%) in the radiative heating rate was predicted for the Venusian case. However, the magnitude of the measured radiation showed a large scatter and did not agree well with the theoretical predictions, even in the equilibrium region. Arnold et al.[18,22] observed the nonequilibrium radiation overshoot phenomenon for CN in CO_2-N_2 mixtures, but did not determine the equilibration distance or quantify the extent of radiation enhancement due to nonequilibrium. In addition, there are measurements made in shock tubes of the rate coefficients of reactions involving most of the constituent species of the Martian atmosphere.[9,10,23-43]

From these studies, one concludes that the thickness of the relaxation zone behind the shock wave formed over a blunt body flying into the Martian atmosphere and the nonequilibrium radiation produced therein are currently uncertain. The existing theoretical predictions differ, and experimental data are scarce. Furthermore, the few experiments that were conducted did not simulate the Martian atmosphere well. The first purpose of the present work is to derive a set of thermochemical relaxation rate parameters and chemical reaction rate coefficients which could explain the few relevant experiments. Secondly, the present work attempts to assess the impact of the thermochemical nonequilibrium phenomena on radiative heating rates for the stagnation point of the Martian entry vehicle.

The present work is a continuation of the work started in Ref. 44 in which the same problem was investigated for superescape velocity entries into the Earth's atmosphere, and uses the same methodology used therein. Some of the details missing in the present work can be found therein.

Thermochemical Model

Thermochemical Nonequilibrium Phenomena

It has been known in recent years that the flow behind a bow shock wave formed over a blunt body entering a planetary atmosphere at a high speed in a low density regime

tends to be in a thermochemical nonequilibrium state, in which the electron thermal temperature and the vibrational and electronic excitation temperatures are different from the translational temperature of the heavy particles.[45-48] The past work on this subject led to the development of a two-temperature model and a computer code named NONEQ (nonequilibrium) which implements this model for a one-dimensional flow.[49] In this code, T_v is calculated independently of T. Relaxation of T_v is calculated allowing for several phenomena that occur only at very high postshock temperatures. The rate coefficients of the dissociation reactions occurring in this environment are assumed to be a function of the geometric average temperature

$$T_a = \sqrt{TT_v} \tag{1}$$

In the NONEQ code, the flow properties are calculated for a one-dimensional flow in a constant-area duct, such as in a shock tube, and along the stagnation streamline over a blunt body through a transposition of the constant-area solutions.[6] The same thermochemical model is incorporated into an axisymmetric two-dimensional code in Ref. 17. Radiation phenomena are calculated for such a nonequilibrium environment in the NONEQ code using a line-by-line technique. The present study is carried out using these codes.

Characterization of Induction Phenomena

Millikan and White[7] have shown that τ_v for most gases can be expressed by

$$p\tau_v = \exp[a(T^{-1/3} - b) - 18.42] \quad \text{atm s} \tag{2}$$

They show also that the parameters a and b can be expressed for many gases by the simple expressions

$$a = 0.00116\mu^{0.5}\theta^{1.333}, \qquad b = 0.015\mu^{0.25} \tag{3}$$

where μ is the equivalent molecular weight between the two colliding particles in g/mol, and θ is the characteristic vibrational temperature (the vibrational constant ω_e divided by the Boltzmann constant) in deg K.

Due to the thermal nonequilibrium mentioned above, dissociation reactions are preceded by a period of induction or incubation behind a shock wave. At relatively low shock speeds (less than about 4 km/s in air or nitrogen), the induction time was found to be about equal to τ_v given by the above equation. However, at higher shock speeds, the induction times were found to become longer, contrary to the general behavior of τ_v.[50] This behavior is attributed in the two-temperature model to the diffusive nature of vibrational relaxation and collision-limiting of vibrational excitation (see Chap. 3 of Ref. 48). The vibrational excitation rate cannot be larger than that corresponding to the elastic collision cross section. This phenomenon is accounted for by adding to the vibrational relaxation time the time for the elastic collisions in the form[6,45-48]

$$\tau(\text{total}) = \tau_v + [n_t\sqrt{(8kT/\pi m)}\sigma_v]^{-1} \tag{4}$$

The quantity σ_v is represented by[6,45-48]

$$\sigma_v = \sigma_v'(50{,}000/T)^2 \quad \text{cm}^2 \tag{5}$$

The value of σ_v' is chosen to fit the existing experimental data.

Since the Martian atmosphere consists of CO_2, N_2, and Ar, and since the degree of ionization is expected to be low in the environment of interest (entry velocity below 9 km/s), the collision encounters that need to be considered in the calculation of vibrational relaxation are those of N_2, CO and CO_2 with Ar, N, O, C, N_2, CO, and CO_2. Of these, the most important is the CO + CO and CO + O encounters, because CO_2 dissociates rapidly into CO + O. Appleton et al.[26] determined the induction times of CO dissociation by monitoring the concentration of oxygen atoms using the resonance absorption technique behind a shock wave. The measured induction times were compared with those predicted by the Millikan-White formula. The experimental data and the predicted values are reproduced in Fig. 1. In the figure, the open circles represent the experimentally observed induction times, while the open triangles indicate the induction times calculated using the Millikan-White formula for each of the experimental points. As seen in the figure, the CO induction times are considerably longer than those given by the Millikan-White formula. In order to reproduce these experimental data, the σ_v' value is varied in the present calculation using the NONEQ code. The calculation requires the rate coefficients for the CO dissociation reactions. The details of the reaction kinetics are given in the following paragraphs. Through this calculation, the best fit was found with a σ_v' value of 3×10^{-18} cm^2 for the CO-CO encounter. In Fig. 1, the results of the present calculations are shown for comparison. The three calculated points in the figure correspond to, in the order of increasing temperature, ρ_1 (preshock density) = 6.6×10^{-5} g/cm^3, U_s = 2.9 km/s, CO concentration = 5%; ρ_1 = 1.45×10^{-5} g/cm^3, U_s = 3.5 km/s, CO concentration = 2%; and ρ_1 = 3.3×10^{-6} g/cm^3, U_s = 4.12 km/s, CO concentration = 2%, respectively.

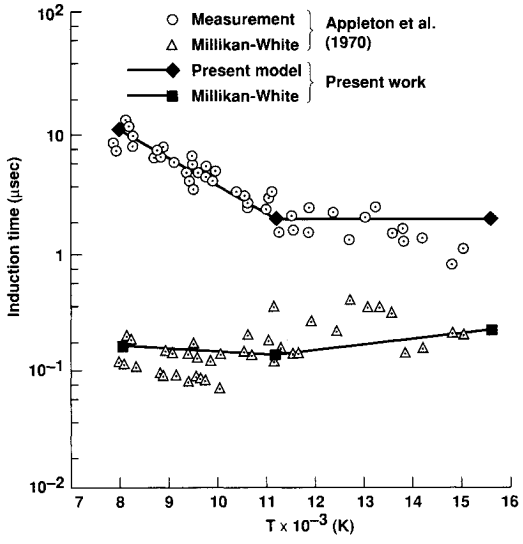

Fig. 1 Comparison between the induction times for CO dissociation measured by Appleton et al.[26] and those predicted by the present model.

The vibrational relaxation behavior in CO_2 has been studied by Camac to a temperature of about 6000 K.[8] In this experiment, radiation emanating from CO_2 at 43,000 Å was monitored. The experiment yielded a and b values of 36.5 and −0.0193, respectively, for the CO_2-CO_2 encounter. There is no experimental data from which the σ_v' can be deduced for CO_2. It was chosen here arbitrarily to be 10^{-16} cm^2. The choice of σ_v' is conservative in that it results in a negligibly small incubation time for CO_2 dissociation. The vibrational relaxation parameters chosen for the species of interest are summarized in Table 1. The vibrational relaxation times calculated by the present model are compared with the experimental data[7,8,51-53] in Fig. 2.

Reaction Model

The shock layer flow over a blunt body entering the Martian atmosphere will dissociate and partially ionize, resulting in the following species: Ar, C, N, O, C_2, N_2, O_2, CN, CO, NO, CO_2, NCO, Ar^+, C^+, N^+, O^+, C_2^+, N_2^+, O_2^+, CN^+, CO^+, NO^+, and e^-. Of particular interest in the present study is the concentration of CO, which emits strong radiation by its

Table 1 Vibrational constants for N_2, CO, and CO_2

	a	b	Source
$N_2(\sigma'_v = 3 \times 10^{-17}$ cm^2 [45]			
M = Ar	240	0.0302	Eq. (3)
N	180	0.0262	Eq. (3)
O	72.4	0.0150	Fitted to Ref. 51
C	72.4	0.0150	Assumed to be same as for N_2-O
N_2	221	0.0290	Eq. (3)
CO	221	0.0290	Eq. (3)
CO_2	245	0.0305	Eq. (3)
CO ($\sigma'_v = 3 \times 10^{-18}$ cm^2, this work)			
M = Ar	215	0.0302	Eq. (3)
N	47.7	0.050	Assumed to be same as for CO-O
O	47.7	0.050	Ref. 53
C	47.7	0.050	Assumed to be same as for CO-O
N_2	198	0.0290	Eq. (3)
CO	198	0.0290	Eq. (3)
CO_2	218	0.0305	Eq. (3)
CO_2 ($\sigma'_v = 10^{-16}$ cm^2, this work)			
M = Ar	50.3	0.0321	Eq. (3)
N	35.8	0.0271	Eq. (3)
O	37.6	0.0278	Eq. (3)
C	33.7	0.0263	Eq. (3)
N_2	45.4	0.0305	Eq. (3)
CO	45.4	0.0305	Eq. (3)
CO_2	36.5	−0.0193	Fitted to Ref. 8

The quantity σ'_v is the limiting cross section for vibrational excitation at 50,000 K. M is the colliding species.

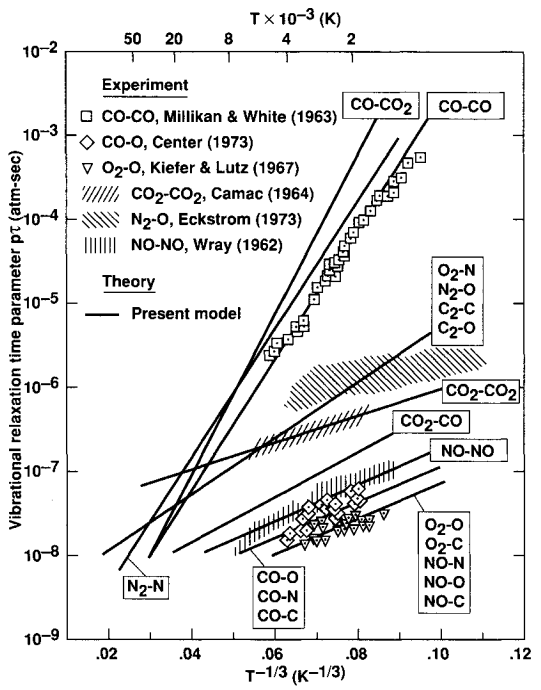

Fig. 2 Comparison between the measured vibrational relaxation times[7,8,51–53] and the present model for carbon-containing species.

"fourth positive" (4+) system; that of CN, which radiates in its "violet" and "red" systems; that of C_2, which emits in its Swan system; and those of C and O, which emit over a wide range of wavelengths, but most strongly in the vacuum-uv region. Of these possible species, Ar^+, N^+, C_2^+, N_2^+, and CN^+ can be eliminated for the reason that their concentrations will be very small and that they will not play any significant role in the rate processes.

Consideration of abundance and heats of formation of these species leads to the conclusion that the reactions that most significantly absorb energy are the dissociation reactions of CO_2 and CO

$$CO_2 + M \rightarrow CO + O + M - 126 \text{ kcal/mol} \quad (6)$$

$$CO + M \rightarrow C + O + M - 256 \text{ kcal/mol} \quad (7)$$

These two reactions are aided by the exchange reactions

$$CO_2 + O \rightarrow CO + O_2 - 8 \text{ kcal/mol} \quad (8)$$

$$CO + O \rightarrow C + O_2 - 138 \text{ kcal/mol} \quad (9)$$

which augment the dissociation rates once a pool of atomic species has been produced. Because of the large disparity in bond energies, CO_2 dissociation is expected to be finished much sooner than CO dissociation. Therefore, establishment of chemical equilibrium is dictated mostly by reactions (7) and (9). For this reason, the accuracy of the rate coefficients for reactions (6) and (8) is not important.

The molecule CN is produced mostly by the exchange reactions

$$CO + N \rightarrow CN + O - 78 \text{ kcal/mol} \quad (10)$$

$$N_2 + C \rightarrow CN + N - 47 \text{ kcal/mol} \quad (11)$$

and removed by

$$CN + O \rightarrow NO + C - 28 \text{ kcal/mol} \quad (12)$$

while the molecule C_2 is produced mostly by

$$CO + C \rightarrow C_2 + O - 114 \text{ kcal/mol} \quad (13)$$

$$CN + C \rightarrow C_2 + N - 36 \text{ kcal/mol} \quad (14)$$

These mechanisms cause an overshoot of the concentrations of the molecules CN and C_2, because the equilibration of these

species is controlled by the slower thermal dissociation reactions

$$CN + M \rightarrow C + N + M - 178 \text{ kcal/mol} \quad (15)$$

$$C_2 + M \rightarrow C + C + M - 142 \text{ kcal/mol} \quad (16)$$

Using the reaction rate coefficients given in Refs. 9 and 10 and elsewhere, calculations have been made in the present work to compare the rates of the four- and five-atom exchange reactions involving CO_2 and NCO. The result shows that most such reactions are as fast as the three-atom reactions, except the reaction

$$N_2 + CO \rightarrow NCO + N - 178 \text{ kcal/mol}$$

This reaction is neglected in the reaction scheme.

There are seven possible associative ionization reactions:

$$C + C \rightarrow C_2^+ + e^- - 138 \text{ kcal/mol}$$

$$N + N \rightarrow N_2^+ + e^- - 133 \text{ kcal/mol}$$

$$O + O \rightarrow O_2^+ + e^- - 159 \text{ kcal/mol}$$

$$C + N \rightarrow CN^+ + e^- - 146 \text{ kcal/mol}$$

$$C + O \rightarrow CO^+ + e^- - 66 \text{ kcal/mol}$$

$$N + O \rightarrow NO^+ + e^- - 63 \text{ kcal/mol}$$

$$CO + O \rightarrow CO_2^+ + e^- - 190 \text{ kcal/mol}$$

Concentrations of the molecular ions produced by these reactions are usually very small, and therefore the reactions can be ignored totally if it were not for the fact that they initiate ionization of atomic carbon, C. Atomic carbon has a fairly low ionization potential. The species C^+ is produced mostly by the electron-impact ionization

$$C + e^- \rightarrow C^+ + e^- + e^- - 260 \text{ kcal/mol}$$

However, in order for this reaction to be started, a finite concentration of electrons is required. The initial electrons are furnished by the associative ionization processes. Based on the abundance of the reactants and the energies required for the processes, it was judged that the reactions $N + O \rightarrow NO^+ + e^-$, $C + O \rightarrow CO^+ + e^-$, and $O + O \rightarrow O_2^+ + e^-$ are the most dominant reactions, and therefore only these three are retained in the scheme.

While there are many charge-exchange processes possible in this gas mixture, the most important of these reactions are those that transfer the charge to C, for the reason given above. Since CO^+, NO^+, and O_2^+ are the first ions to form, the most important charge-exchange reactions are

$$CO^+ + C \rightarrow CO + C^+ + 62 \text{ kcal/mol} \quad (17)$$

$$NO^+ + C \rightarrow NO + C^+ - 46 \text{ kcal/mol} \quad (18)$$

$$O_2^+ + C \rightarrow O_2 + C^+ + 19 \text{ kcal/mol} \quad (19)$$

Reaction Rate Coefficients

In order to deduce the unknown rate parameters, thermodynamic properties and resulting radiation characteristics are calculated using the NONEQ code with the assumed vibrational and reaction rate parameters for a given experimental condition. The radiation characteristics calculated in this way are compared with the experimental data. If they disagree, the parameters most sensitively affecting the observed radiation are varied, until a best match between the experimental data and the calculation is achieved. It is customary to represent the coefficient of a chemical reaction in the form

$$k_f = CT_x^n \exp(-T_d/T_x) \quad \text{cm}^3 \text{ mol}^{-1} \text{ s}^{-1} \quad (20)$$

where T_x is the temperature controlling the reaction. In the two-temperature environment of concern, T_x is taken to be T_a for dissociation reactions, T_v for all reactions where an electron is a reactant, and T for the rest. The final set of reaction rate coefficients selected through this process is presented in Table 2. In the following, this process is explained.

Ionic Reactions

All three atomic species, C, N, and O, undergo electron-impact ionization. However, since the concentration of N is much smaller than those of the other two species, the electron-impact ionization of N is ignored. The C and n values for the electron-impact ionization of carbon atom are assumed to be the same as those for oxygen, which are in turn deduced from those for nitrogen (see Chap. 8 of Ref. 48). The recombination rate coefficient so determined is nearly the same as that obtained by Dunn.[23]

Radiative recombination will occur also for all three atomic species, but again, since the concentration of N^+ is very small, the process $N^+ + e^- \rightarrow N + h\nu$ is ignored. The rate coefficient for $C^+ + e^-$ recombination is calculated using the computer code NONEQ using the data provided with the code (the code has an option which, when exercised, gives the radiative recombination rate coefficients). The data in NONEQ had been obtained from the theoretical work of Griem.[54]

CO_2 Dissociation

Among the neutral reactions, the reactions of first interest are those of CO_2 decomposition, reactions (6) and (8), because they are the first chemical reactions to occur behind a shock wave. Of interest is the rate coefficient for dissociation, reaction (6), because that is the rate-limiting reaction. Reference 9 provides a review of the existing rate coefficient data on this reaction as of 1986. Since the review, one more set of data has been produced by Burmeister and Roth.[25] These data are shown in an Arrhenius plot in Fig. 3. Of particular interest is the data by Davies[24] which is the only set of data that covers the temperature range above 4000 K.

One apparent feature of the dissociation rate of CO_2 is that the exponent n is a relatively large negative value. In the two-temperature model used here, any such behavior is attributed to the low vibrational temperature in the dissociation zone[55]: it is shown in Ref. 55 that such a behavior can be numerically recreated in the two-temperature model using a relatively small negative n value. For N_2 and O_2 dissociation, the n value appropriate to the two-temperature model was seen to be between -1 and -1.6. In the present work, the n value for CO_2 dissociation is chosen arbitrarily to be -1.5. The choice of this value is immaterial, as will become apparent later.

The rate coefficient C value for the case where the third body, M, is Ar, is taken to be 6.9×10^{20} which gives a k_f value that agrees with the data by Davies[24] at $T = 5000$ K. Based on the discussion given in Ref. 9, the C values for the cases where the third body is a molecule are assumed to be 10 times that for M = Ar. Those for the cases where the third body is an atom is taken arbitrarily to be 15 times that for M = Ar, because atoms are usually more efficient than molecules. These values are compared with the existing data in Fig. 3.

The validity of the CO_2 dissociation rate coefficient value for M = Ar is verified by comparing the calculated radiation behavior with the experimental data by Davies.[24] In this experiment, the infrared radiation at 29,000 Å was measured in a 1% CO_2-99% Ar mixture in the reflected-shock region of

Table 2 Reaction rate coefficients for Martian atmosphere (present model)

Reaction	M	T_x	C	n	T_d	Source
Dissociation reactions						
$C_2 + M \rightarrow C + C + M$	All	T_a	3.7^{14}	0.00	69,900	Ref. 38
$N_2 + M \rightarrow N + N + M$	Ar	T_a	7.0^{21}	−1.60	113,200	Ref. 47
	C		3.0^{22}			
	N		3.0^{22}			
	O		3.0^{22}			
	C_2		7.0^{21}			
	N_2		7.0^{21}			
	O_2		7.0^{21}			
	CN		7.0^{21}			
	CO		7.0^{21}			
	NO		7.0^{21}			
	CO_2		7.0^{21}			
	e^-		1.2^{25}			Ref. 44
$O_2 + M \rightarrow O + O + M$	Ar	T_a	2.0^{21}	−1.50	59,750	Ref. 47
	C		1.0^{22}			
	N		1.0^{22}			
	O		1.0^{22}			
	C_2		2.0^{21}			
	N_2		2.0^{21}			
	O_2		2.0^{21}			
	CN		2.0^{21}			
	CO		2.0^{21}			
	NO		2.0^{21}			
	CO_2		2.0^{21}			
$CN + M \rightarrow C + N + M$	All	T_a	2.5^{14}	0.00	71,000	Ref. 34
$CO + M \rightarrow C + O + M$	Ar	T_a	2.3^{19}	−1.0	129,000	This work
	C		3.4^{20}			
	N		3.4^{20}			
	O		3.4^{20}			
	C_2		2.3^{20}			
	N_2		2.3^{20}			
	O_2		2.3^{20}			
	CN		2.3^{20}			
	CO		2.3^{20}			
	NO		2.3^{20}			
	CO_2		2.3^{20}			
$NO + M \rightarrow N + O + M$	Ar	T_a	5.0^{15}	0.00	75,500	Ref. 47
	C		1.1^{17}			
	N		1.1^{17}			
	O		1.1^{17}			
	C_2		5.0^{15}			
	N_2		5.0^{15}			
	O_2		5.0^{15}			
	CN		5.0^{15}			
	CO		5.0^{15}			
	NO		1.1^{17}			
	CO_2		1.1^{17}			
$CO_2 + M \rightarrow CO + O + M$	Ar	T_a	6.9^{20}	−1.50	63,275	This work
	C		1.4^{22}			
	N		1.4^{22}			
	O		1.4^{22}			
	C_2		6.9^{21}			
	N_2		6.9^{21}			
	O_2		6.9^{21}			
	CN		6.9^{21}			
	CO		6.9^{21}			
	NO		6.9^{21}			
	CO_2		6.9^{21}			
$NCO + M \rightarrow CO + N + M$	All	T_a	6.3^{16}	−0.5	24,000	Ref. 35
Neutral exchange reactions						
$NO + O \rightarrow N + O_2$		T	8.4^{12}	0.00	19,450	Ref. 47
$N_2 + O \rightarrow NO + N$		T	6.4^{17}	−1.00	38,370	Ref. 47
$CO + O \rightarrow C + O_2$		T	3.9^{13}	−0.18	69,200	Ref. 30
$CO + C \rightarrow C_2 + O$		T	2.0^{17}	−1.00	58,000	This work
$CO + N \rightarrow CN + O$		T	1.0^{14}	0.00	38,600	This work
$N_2 + C \rightarrow CN + N$		T	1.1^{14}	−0.11	23,200	Ref. 43
$CN + O \rightarrow NO + C$		T	1.6^{13}	0.10	14,600	Ref. 29
$CN + C \rightarrow C_2 + N$		T	5.0^{13}	0.00	13,000	Ref. 34
$CO_2 + O \rightarrow O_2 + CO$		T	2.1^{13}	0.00	27,800	Ref. 39
$CN + O_2 \rightarrow NCO + O$		T	6.6^{12}	0.00	−200	Ref. 423
$CN + CO_2 \rightarrow NCO + CO$		T	4.0^{14}	0.00	19,200	Ref. 29
$CN + NO \rightarrow NCO + N$		T	1.0^{14}	0.00	21,200	Ref. 31
$CO + NO \rightarrow NCO + O$		T	3.8^{17}	−0.873	51,600	Ref. 36
$CN + CO \rightarrow NCO + C$		T	1.5^{16}	−0.487	65,800	Ref. 36

Table 2 (*Continued*)

Reaction	M	T_x	C	n	T_d	Source
Associative ionization reactions						
$N + O \rightarrow NO^+ + e^-$		T	8.8^8	1.00	31,900	Ref. 44
$O + O \rightarrow O_2^+ + e^-$		T	7.1^2	2.70	80,600	Ref. 44
$C + O \rightarrow CO^+ + e^-$		T	8.8^8	1.00	33,100	This work
Charge exchange reactions						
$NO^+ + C \rightarrow NO + C^+$		T	1.0^{13}	0.00	23,200	This work
$O_2^+ + O \rightarrow O^+ + O_2$		T	4.0^{12}	−0.09	18,000	Ref. 47
$NO^+ + N \rightarrow O^+ + N_2$		T	3.4^{13}	−1.08	12,800	Ref. 47
$NO^+ + O \rightarrow O_2^+ + N$		T	7.2^{12}	0.29	48,600	Ref. 47
$CO + C^+ \rightarrow CO^+ + C$		T	1.0^{13}	0.00	31,400	This work
$O_2 + C^+ \rightarrow O_2^+ + C$		T	1.0^{13}	0.00	9,400	This work
Electron-impact ionization reactions						
$C + e^- \rightarrow C^+ + e^- + e^-$		T_v	3.9^{33}	−3.78	130,700	This work
$O + e^- \rightarrow O^+ + e^- + e^-$		T_v	3.9^{33}	−3.78	158,500	This work
Radiative recombination reactions						
$O^+ + e^- \rightarrow O + h\nu$		T_v	1.07^{11}	−0.52		This work
$C^+ + e^- \rightarrow C + h\nu$		T_v	2.02^{11}	−0.46		This work

T_x is the controlling temperature, C is in cm^3 mole^{-1} s.$^{-1}$

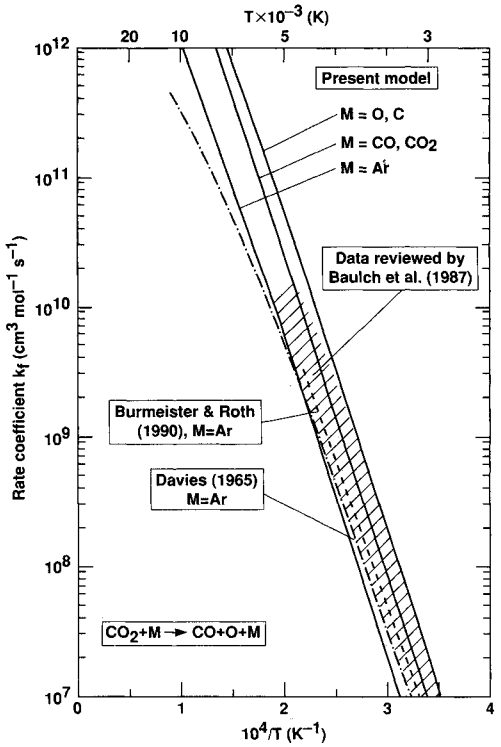

Fig. 3 Comparison between the dissociation rate coefficient for CO_2 selected in the present work and the existing experimental data.[9,24,25]

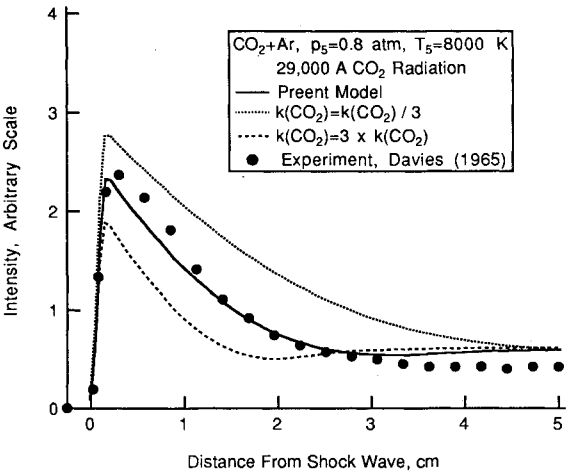

Fig. 4 Comparison between the experimental data on the 29,000 A radiation in CO_2-Ar mixture[24] and the present calculation; reflected-shock conditions: p_5 = 0.8 atm, T_5 = 8000 K.

a shock tube. In Fig. 4, the calculated results are compared with the experimental data. The present model reproduces the experimental data closely. For comparison, the calculations made with the CO_2 dissociation rate coefficients divided by and multiplied by 3 are shown. As seen here, these alternate rate coefficients lead to erroneous predictions of the intensity of the infrared radiation.

CO Dissociation

Reference 9 provides a thorough review of the existing rate coefficient data for CO decomposition, reactions (7) and (9). Since the review, one more set of data has been produced by Mick and Roth.[28] Of interest is the rate of CO dissociation, reaction (7), because the rate coefficient for reaction (9) is relatively well known.[9] Following the logic given above, the n value for this process is chosen arbitrarily to be −1. The C value for M = Ar is chosen so that the k_f value would agree with the data of Mick and Roth at 10,000 K. Again, based on the discussions given in Ref. 9, the C values for M = molecules are taken to be 10 times the argon value. The C values for M = atoms are taken to be 15 times the argon value. The values chosen in the present work are compared with the existing experimental data in Fig. 5.

The validity of the presently selected rate coefficient values for CO dissociation is tested against the experimental data of Nealy and Haggard.[20] In this experiment, the radiation at 1580 Å from the CO 4+ system was measured in a shock tube with 100% CO_2 flow at a shock velocity of 9 km/s. At this shock speed, CO_2 dissociates immediately behind the shock wave, and CO dissociation occurs. Therefore, intensity of this radiation is dictated mostly by the rate of dissociation of CO and T_v of the flow. The vibrational-electron-electronic temperature is affected directly by the a, b, and σ_v' values for CO, and indirectly by the dissociation rate coefficient for CO. For this reason, this experimental data offers a valid test of the CO dissociation model. In Fig. 6, the results of present calculations are compared with the experimental data. In the figure, the ordinates represent the intensity of radiation observed at the wall in the direction normal to the flow integrated over a wavelength interval of 4 Å at around 1580 Å. The diameter of the shock tube over which the intensity is integrated was 15 cm. As seen in the figure, the present model agrees fairly well with the experiment. The figure also shows the calculations made using different rate coefficients for CO dissociation, reaction Eq. (7).

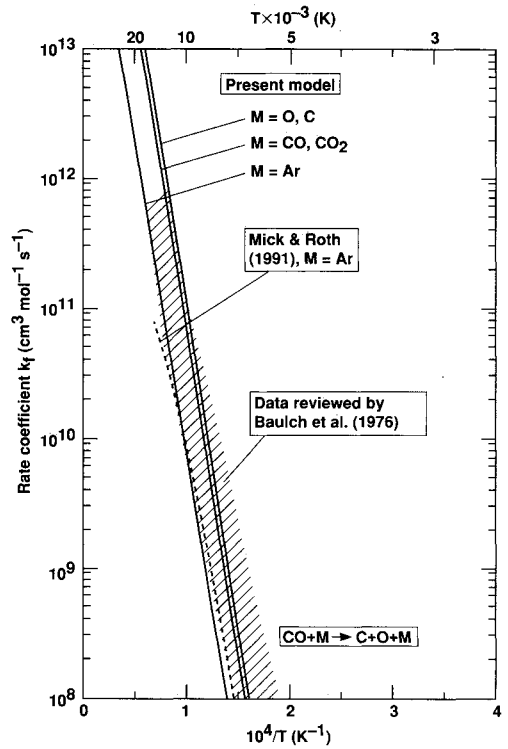

Fig. 5 Comparison between the dissociation rate coefficient for CO selected in the present work and the existing experimental data.[9,28]

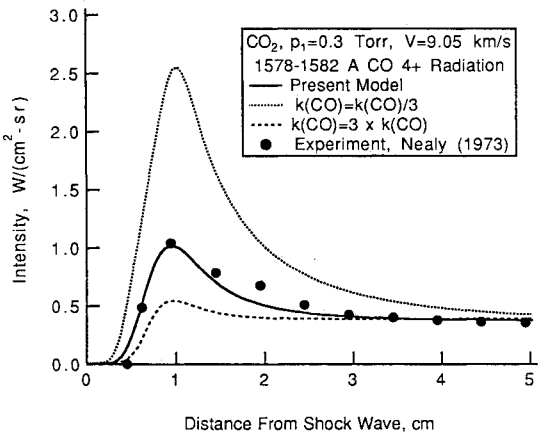

Fig. 6 Comparison between the experimental data on the 1580 Å CO fourth positive band radiation in CO_2[21] and the present calculation; p_1 = 0.3 Torr, V = 9.05 km/s.

$CO + C \rightarrow C_2 + O$ *(C_2 Formation) Reaction*

The rate processes of next importance are those of the C_2 formation, reactions (13) and (14), because C_2 is a major radiator (see the section on Radiation). Of these two processes, reaction (13) is dominant over (14) in the environment of interest. Unfortunately, no rate coefficient data exists for reaction (13). The rate coefficient for this reaction is determined in the present work by comparing with the experiment of Hanson.[27] In that experiment, the C_2 Swan band radiation at 5000 Å was measured in a shock tube in 100% CO. The intensity variation in this experiment is determined mostly by the magnitude of reaction (13). Through a process of trial and error, the rate coefficient value is selected in the present work to be

$CO + C \rightarrow C_2 + O$:

$$k_f = 2.0 \times 10^{17} T^{1} \exp(-58{,}000/T) \quad \text{cm}^3 \text{ mole}^{-1} \text{ s}^{-1}$$

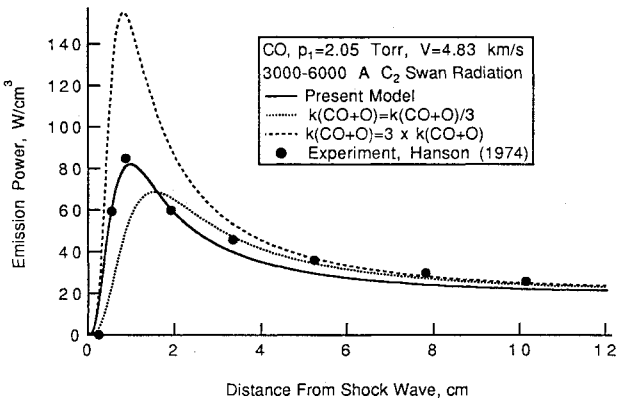

Fig. 7 Comparison between the experimental data on the 4800 Å C_2 Swan band radiation in CO[27] and the present calculation; p_1 = 2.05 Torr, V = 4.83 km/s.

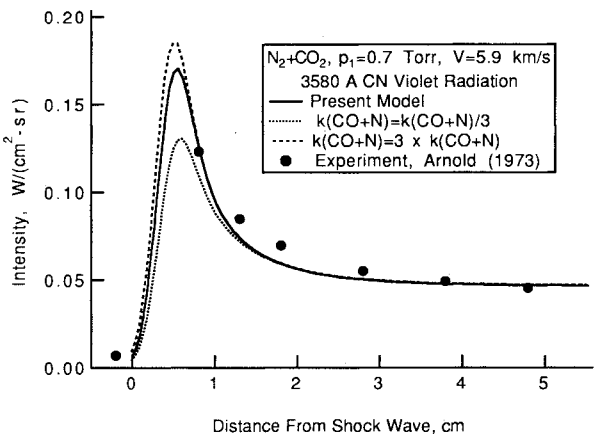

Fig. 8 Comparison between the experimental data on the 3580 Å CN violet band radiation in 24% CO_2-76% N_2 mixture[22] and the present calculation; p_1 = 0.70 Torr, V = 5.9 km/s.

The intensity of the C_2 Swan radiation calculated using this rate coefficient, and those obtained using the rate coefficients $\frac{1}{3}$ and 3 times this value, are compared with the experimental data in Fig. 7.

$CO + N \rightarrow CN + O$ *and* $N_2 + C$ *(CN Formation) Reaction*

The rate processes of next importance are those that produce CN, reactions (10) and (11). The rate coefficient for the reverse reaction to reaction (10) has been determined in Refs. 10, 29, 36, 37, and 40. The forward reaction rate coefficients are deduced from these data invoking the detailed balancing principle under equilibrium. The averages of these are

$CO + N \rightarrow CN + O$:

$$k_f = 10^{14} \exp(-38{,}600/T) \quad \text{cm}^3 \text{ mole}^{-1} \text{ s}^{-1}$$

The rate coefficient for reaction (11) has been determined in Ref. 43. The rate coefficient for the reverse reaction to reaction (11) has been measured in Refs. 29, 33, 34, and 41. In the present work, the value of Ref. 43

$N_2 + C \rightarrow CN + N$:

$$k_f = 1.11 \times 10^{14} T^{-0.11} \exp(-23{,}200/T) \quad \text{cm}^3 \text{ mole}^{-1} \text{ s}^{-1}$$

is used.

The validity of these rate coefficient values is tested against the experiment of Arnold and Nicholls.[22] In this experiment, the intensity of the CN violet band at around 3883 Å is measured in a mixture of 24% CO_2-76% N_2. In Fig. 8, the intensity

values calculated using the rate coefficients so deduced are compared with the measured values. For the purpose of comparison, the figure also shows the calculation made using the rate coefficient values three times larger and smaller than the chosen value. Unfortunately, in the region of peak radiation where calculations show difference, experimental data are absent (out of scale). However, based on what is available, radiation intensity is judged to be relatively insensitive to the value of the rate coefficient. The value chosen in the present work is at least consistent with the experimental data.

Associative Ionization Reaction

Among the three associative ionization reactions considered, the rate coefficients for the associative ionization reactions $N + O \rightarrow NO^+ + e^-$ and $O + O \rightarrow O_2^+ + e^-$ are taken from Ref. 44. The rate coefficient for the reaction $C + O \rightarrow CO^+ + e^-$ is taken to be the same as that for the N + O reaction.

Charge Exchange Reactions

Six charge exchange reactions listed in Table 2 are considered in the present work. The possible seventh, $CO^+ + O \rightarrow CO + O^+$ is not considered because it will be slow compared with the competing reaction $CO^+ + C \rightarrow CO + C^+$. For the reactions involving nitrogen or oxygen species only, the rate coefficients are taken from Ref. 47. The rate parameters for the reactions containing carbon, which are unknown, are estimated to be $C = 10^{13}$ cm^3 mole^{-1} s^{-1} and $n = 0$. The rate coefficient values so determined are roughly equal to those known rate coefficient values for the nitrogen and oxygen species at 10,000 K.

Behavior of the Flow

Relaxation Distances in Constant-Area Flow

Using the rate parameters determined as described above, the thermodynamic state variables are calculated for the Martian gas mixture for a flow in a constant-area duct using the NONEQ code over the velocity range of 6–9 km/s. The freestream density is varied for each velocity such that the post-shock static pressure p_s, determined through the hypersonic approximation

$$p_s = \rho_\infty V^2 \tag{21}$$

is 0.15 atm. This pressure is chosen arbitrarily. The radiative heat transfer rate to the stagnation point of a Martian entry vehicle becomes maximum typically at this pressure.[56] The results of calculation of flow properties for $V = 8$ km/s are shown in Figs. 9a and 9b.

In Fig. 9a, T is initially 46,200 K behind the shock wave. The two temperatures, T and T_v, become nearly the same at about 0.3 cm behind the shock wave. This rate of equalization between T and T_v for the Martian gas mixture is significantly faster than that in air. This fast equalization of temperatures is believed to be caused partly by the fast vibrational relaxation of CO_2. Even though vibrational excitation of CO is very slow (see Fig. 1), the vibrational temperature is raised significantly by the time CO_2 is decomposed into CO and O. This finding agrees with the conclusions drawn in Refs. 13–17.

In Fig. 9b, one sees that dissociation of CO_2 into CO and O occurs very fast (within 0.1 cm). Dissociation of CO into C and O commences early, but does not reach equilibrium over a long distance. Equilibration of CO dissociation is so slow first because its dissociation energy is large, and second because equilibration of ionization processes is slow. One sees that the ionized species C^+, O^+, NO^+, CO^+ and O_2^+ first undergo an overshoot, and then gradually decay. The process of decay of the ionized species releases energy to the flow so that more of the CO molecules can be dissociated. The ionized

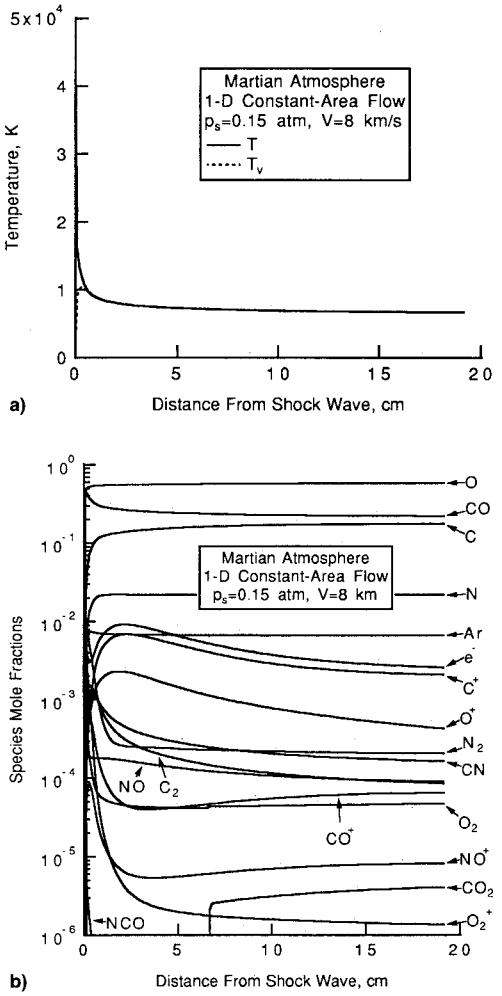

Fig. 9 Thermodynamic state variables in a constant-area duct calculated by the present model for the Martian atmosphere for $V = 8$ km/s, $R = 1$ m, and $p_s = 0.15$ atm: a) temperatures and b) species mole fractions.

species do not reach their respective equilibrium values over the entire length of 20 cm. Though not shown, the steady state is reached at around 40 cm for this case.

As will be shown later, the radiative power emitted by the gas reaches a high peak at around 0.3 cm behind the shock, and declines thereafter. The decline is initially very rapid, but becomes gradual later on. At the distance of 20 cm, the emission power has not yet reached a steady state. The steady state in radiation emission, which is interpreted to be the state of equilibrium, is reached at a distance of about 40 cm for this case.

It is customary to define characteristic relaxation distances or times from the radiation history plot. Two such characteristic values are defined: 1) the distance or time to the peak radiation point (peak radiation point) and 2) those to the point where the radiation intensity falls to 1.1 times the equilibrium value (equilibration point). Since the distances from the shock wave to these points are nearly inversely proportional to the freestream pressures, the product τp_∞, where τ is the time to reach one of those two characteristic points, and p_∞ is the freestream pressure, is very nearly independent of the freestream pressure.

In Fig. 10, the existing experimental data on τp_∞ for CO_2-containing gas mixtures[19,21,22,24] are presented and compared with those for air.[6] In the figure, the experimental data by Thomas and Menard[19] had been obtained using CO_2-N_2 mixture ratios that varied over a wide range. The experimental data were not sufficiently precise to differentiate by mixture ratio. The figure indicates that the peak radiation times de-

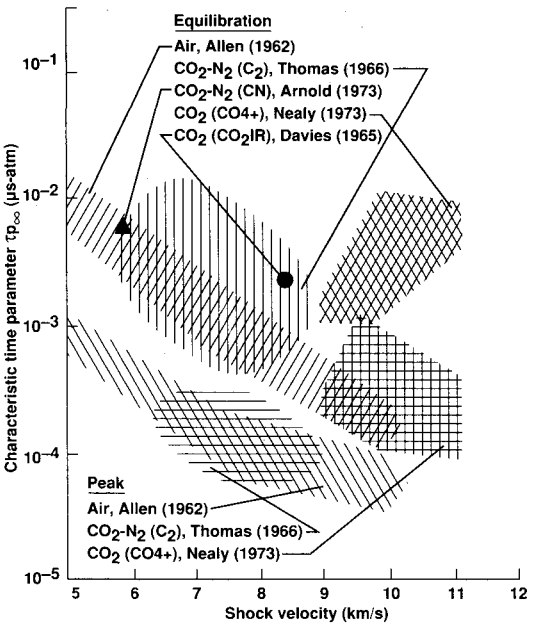

Fig. 10 Comparison between the measured characteristic relaxation times for the CO_2-containing gas mixture[19,20,22,24] and those for air.[47]

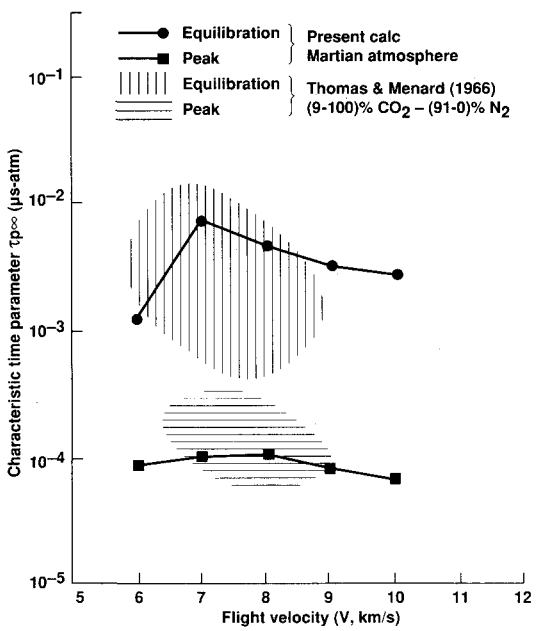

Fig. 11 Comparison between the characteristic relaxation times predicted by the present model based on relaxation behavior of the C_2 Swan radiation and the existing experimental data.[19]

termined by Thomas and Menard for the CO_2-N_2 mixture are approximately the same as those obtained in air. However, the similar measurement by Nealy with the 4+ system of CO in 100% CO_2 give discernibly larger times, though at different flow velocities. The same trend is true for the equilibration time: Nealy's values are larger than Thomas-Menard's values. The Thomas-Menard values for the equilibration time are slightly larger than those for air. The equilibration distance determined by Arnold and Nicholls[22] and by Davies[24] fall within the range of those by Thomas and Menard, even though the methods used are different.

The peak and the equilibration times are calculated in the present work using the NONEQ code, and are compared with the experimental data of Thomas and Menard[19] in Fig. 11. As seen here, the calculated peak radiation times pass through approximate midpoints of the experimental data. However,

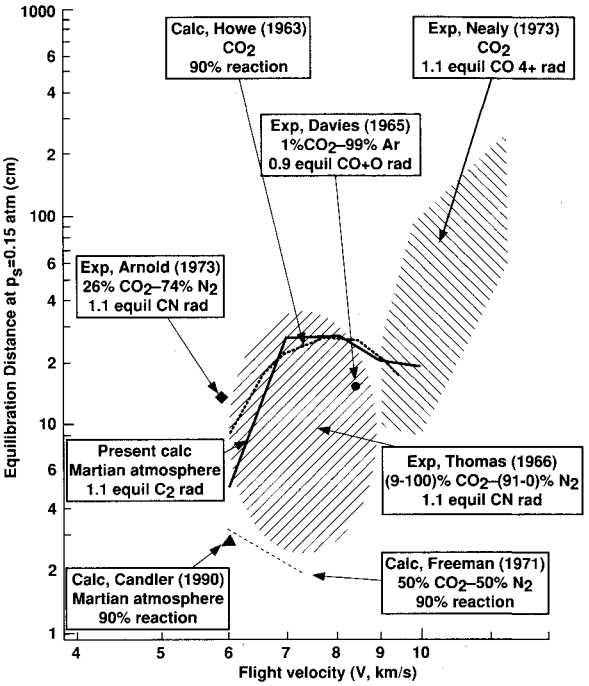

Fig. 12 Comparison between the equilibration distance at p_s = 0.15 atm in Martian atmosphere predicted by the present model and the existing experimental data[19,20,22,24] and other theoretical predictions.[13,16,17]

the experimental data for the equilibration point are not sufficiently precise to render judgment on the accuracy of the calculation.

In Fig. 12, the calculated equilibration distances are shown and compared with the experimental data and other theoretical predictions for p_s = 0.15 atm. The theoretical predictions are those by Howe et al.,[13,14] Freeman and Oliver,[16] and Candler.[17] In those calculations, the equilibration distance was considered to be the point where the reactions are 90% complete in these theoretical predictions. The present prediction is seen to agree approximately with the experimental data of Arnold and Nicholls[22] and of Davies.[24] It is larger than the mean value of the experimental data of Thomas and Menard, and approaches the mean value of Nealy's data. Thus, the present calculation is at least consistent with the existing experimental data, to within the scatter in the existing data. The theoretical prediction by Howe agrees approximately with the present prediction, but those by Freeman and Oliver and by Candler are both considerably smaller. The predicted equilibration distance varies between 5–27 cm, depending on the flow speed. Considering that the shock layer thickness is about 40 cm for a 10-m nose radius, this means that the shock layer flow must be calculated using the nonequilibrium model for body radius smaller than about 10 m.

Flow Along Stagnation Streamline

The flow properties along the stagnation streamline in the shock layer over a hemispherical body are calculated in the present work using both the one-dimensional code NONEQ and the axisymmetric two-dimensional code developed in Ref. 17 using the thermochemical model described above. The two-dimensional calculation is made using 100 mesh points along the direction normal to the body wall. As described in Ref. 6, the NONEQ code is based on the assumption that the shock wave is infinitesimally thin and its location is given, i.e., it uses the so-called thin-shock, shock-fitting approach. The temperature behind the shock is that determined by the ideal-gas Rankine-Hugoniot relationship. The two-dimensional code of Ref. 17 uses the so-called shock-capturing method in which the shock wave is described over a number of grid points,

resulting in a shock wave of finite thickness. A finite-volume approach is made in the two-dimensional method, so that the solution values are represented at the centers of each computing cell. The peak translational temperature appearing in the shock wave is less than the Rankine-Hugoniot value used in the shock-fitting method. In the one-dimensional calculation, the wall is assumed to be noncatalytic to surface reactions. In the two-dimensional calculation, both fully catalytic and noncatalytic walls are considered. The wall temperature is set at 1800 K.

The solutions from the two codes are compared in Figs. 13a and 13b for the case of $R = 1$ m, $p_s = 0.15$ atm, and $V = 8$ km/s. Figure 13a shows that the postshock temperature T in the two-dimensional solution is much lower than that in the one-dimensional solution, for the reason given above. The two temperatures do not approach the given wall temperature of 1800 K because of the finite volume approach taken. The peak vibrational temperature is nearly the same in the two solutions, but its location is different: the peak occurs later in the one-dimensional flow. In this region immediately behind the shock wave, the stagnation streamline flow closely resembles a constant-area flow. Therefore, the difference cannot be attributed to the constant-area nature of the one-dimensional solution. Rather, the difference in the location of the peak in T_v is believed to be due to the difference between the shock-capturing and the shock-fitting method. The assumption of infinitesimally thin shock wave made in the shock-fitting method in the one-dimensional solution is unrealistic. On the other hand, numerical spreading of shock wave in the shock capturing method used in the axisymmetric solution is also troublesome. Identifying the consequences of these differences is beyond the scope of the present work.

In Fig. 13b, the mole fractions of the major species, CO, O, and C, from the two solutions are compared. The two-dimensional solution is that for a fully catalytic wall. As seen here, there is only a small difference between the two solutions. In the two-dimensional solution, CO increases and both O and C decrease near the wall because of the surface catalytic effect.

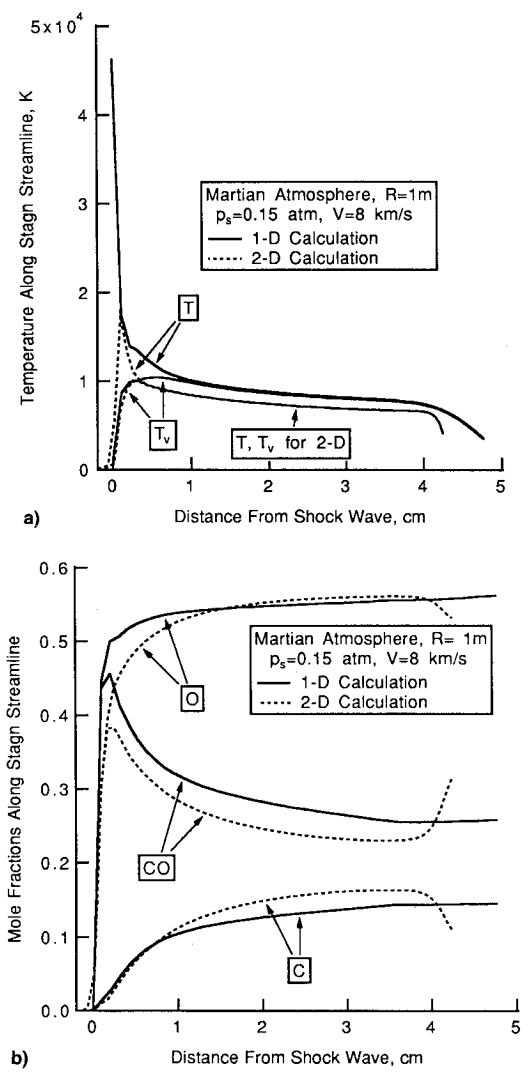

Fig. 13 Comparison between the one-dimensional and two-dimensional calculations of the nonequilibrium thermodynamic properties along the stagnation streamlines of a hemispherical body, $R = 1$ m, at $V = 8$ km/s and $p_s = 0.15$ atm: a) temperatures and b) mole fractions of major species.

Stagnation Point Radiative Heat Fluxes

The stagnation-point radiative heat flux q_r for a hemispherical body flying in a gas mixture containing CO_2 and N_2 has been calculated previously in Refs. 5 and 57, though their relative concentrations were not necessarily those of the Martian atmosphere. Those calculations have been made under the assumption of thermochemical equilibrium in the shock layer and an inviscid flow, neglecting radiative cooling and using the assumption that the rotational lines in molecular bands are smeared. Recently, calculations have been made by Hartung et al.[58] for the Martian gas mixture also assuming an equilibrium inviscid flow, but allowing for radiative cooling and with a detailed description of the profiles of the rotational lines. Hartung et al.'s calculations agree approximately with those of Refs. 5 and 57. The q_r values calculated by Hartung et al. are represented well, at least over a limited range of densities and nose radii, by an analytical expression developed by Tauber and Sutton,[59] which fits the calculation by Hartung et al. and expresses q_r in terms of freestream density, flight velocity, and nose radius.

The spectral part of the program NONEQ allows calculation of radiative transport through a flowfield using a Voigt profile which accounted for four collision-broadening mechanisms (natural broadening, Stark broadening, van der Waals broadening, and resonance broadening). Radiative heat flux is calculated using this code along the stagnation streamline

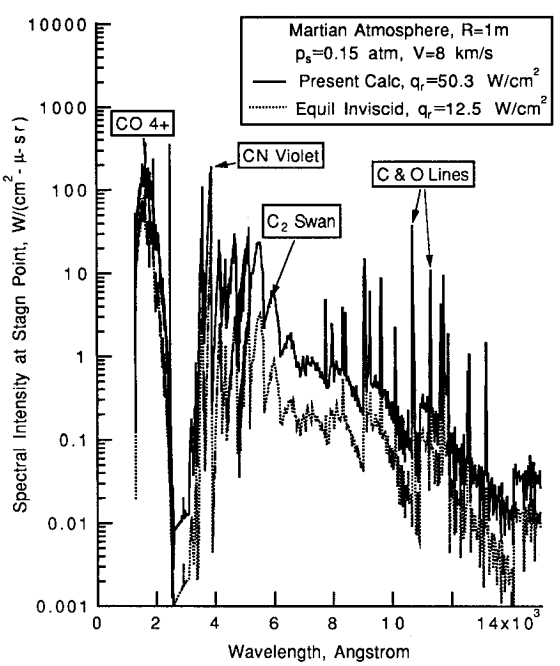

Fig. 14 Comparison between the radiation spectra calculated by the present nonequilibrium model, and for the equilibrium inviscid case at the stagnation point of a body of $R = 1$ m for $p_s = 0.15$ atm and $V = 8$ km/s.

neglecting the effect of radiative cooling or absorption. A typical radiation spectrum obtained by this calculation is shown in Fig. 14. The four major components of radiation, that is, CO 4+ system, CN violet and red systems, C_2 Swan system, and atomic radiation from C and O, are identified in the figure. Other radiation sources are too weak to be of significance. Spectral radiation is strongest at wavelengths below 2000 Å.

The relative contributions of the four main components of radiation are compared in Fig. 15a, which shows emissions, and Fig. 15b, which shows radiative heat fluxes, as a function of distance. For these, flow properties have been obtained from the two-dimensional code. The flow properties are given as inputs to NONEQ to calculate the radiative properties. As seen in Fig. 15a, radiation emission is strongest for the atoms and CO; CN and C_2 radiate much more weakly. All four components peak at a point close to the shock wave, and decay thereafter. According to Fig. 15b, the radiative fluxes for CO and atoms also reach a peak and decay thereafter, indicating that self-absorption is occurring. Self-absorption is particularly strong for atoms. As a result of the self-absorption, the flux due to atoms diminishes to a negligibly small value at the wall. The CO 4+ system also undergoes a substantial self-absorption. Only the fluxes due to CN and C_2 increase monotonically toward the wall. Except for the atomic radiation, there is no discernible absorption in the boundary layer. This is because spectral lines in the boundary layer are very narrow due to low temperature there, and therefore absorption occurs only over the very narrow wavelength range around the line centers.[49] The CO 4+ system dominates the radiative flux reaching the wall.

In Fig. 16, the behavior of radiative flux is shown for R = 10 m. For this case, shock stand-off distance is nearly 40 cm. The nonequilibrium overshoot phenomenon subsides at a distance of about 8 cm behind the shock wave. Beyond 8 cm, flow approaches equilibrium very slowly, and therefore, though not shown, temperature and radiation emission both decrease very slowly. Though the flow should be in equilibrium at the distance of about 30 cm behind the shock for this case (see Fig. 12), the calculated result (not shown) shows that emitted radiation power decreases beyond 30 cm, presumably because of the viscous cooling effect. The changes in temperature and species concentration are so slow that some of the features of radiative transport for a uniform medium are observed here. For instance, the flux from CO 4+ grows approximately as $R^{0.15}$ between the distance of 10–40 cm, which is expected for mostly Gaussian spectral lines. Those from CN and C_2 increase somewhat faster, i.e., by about $R^{0.4}$. This means that the lines in these bands are broadened more by collisions than the CO 4+ band. This is because the extent of collisional broadening is proportional to the square of wavelengths. The atomic radiation from C and O, which occurs mostly in the vacuum-uv wavelengths, and therefore is very Gaussian, does not grow at all, because its very slow growth is offset by the decreasing temperature.

One notes here also that catalyticity of the wall does not significantly affect q_r. As mentioned earlier, calculations have been made with both catalytic and noncatalytic walls. Despite the fact the concentrations of CO molecules in the boundary layer are different between the two cases, little difference was seen in the resulting q_r values. This behavior can be attributed also to the fact that the absorption in the boundary layer occurs only in the very narrow wavelength range around the center of each line.

The calculated q_r values are shown in Fig. 17 for the range of V = 7–9 km/s and R = 1 and 10 m, for p_s = 0.15 atm, and are compared with the equilibrium-inviscid prediction of Tauber and Sutton.[59] As the figure shows, for R = 1 m, the present calculation predicts appreciably stronger radiative flux than the equilibrium-inviscid calculation. This is attributable to the nonequilibrium overshoot phenomena illustrated in Figs. 15a and 15b. However, for R = 10 m, the present value is nearly the same as the equilibrium-inviscid value at V = 7 km/s, and only modestly higher at higher velocities. It is surmised that, for V = 7 km/s and R = 10 m, nonequilibrium overshoot phenomenon is nearly balanced by the absorption

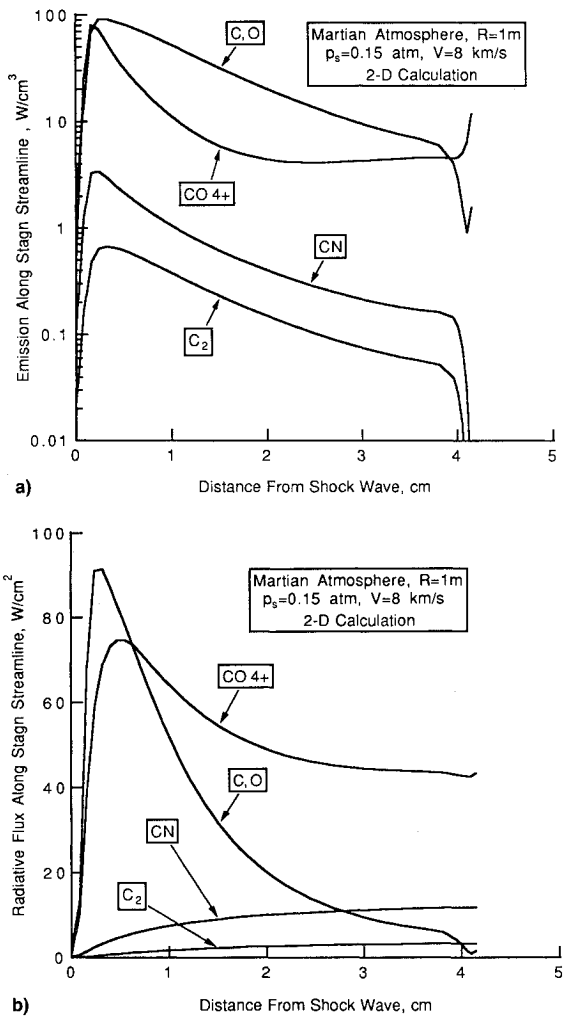

Fig. 15 Radiation characteristics along the stagnation streamline produced by CO 4+, CN, C_2, and C and O atoms for R = 1 m, p_s = 0.15 atm, V = 8 km/s, calculated by the two-dimensional method: a) emission power and b) radiative heat flux.

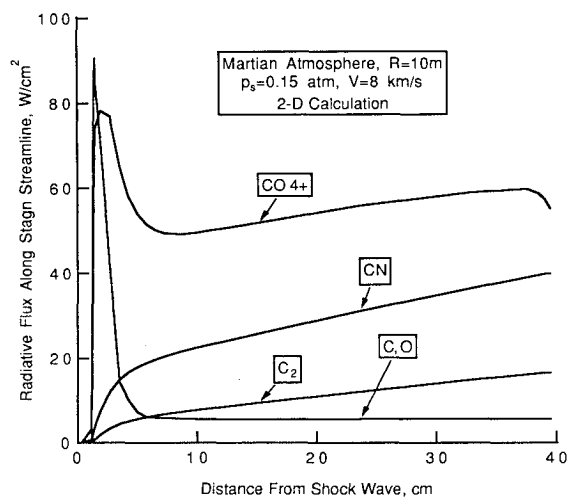

Fig. 16 Radiative heat flux along the stagnation streamline produced by CO 4+ CN, C_2, and C and O atoms for R = 10 m, p_s = 0.15 atm, V = 8 km/s, calculated by the two-dimensional method.

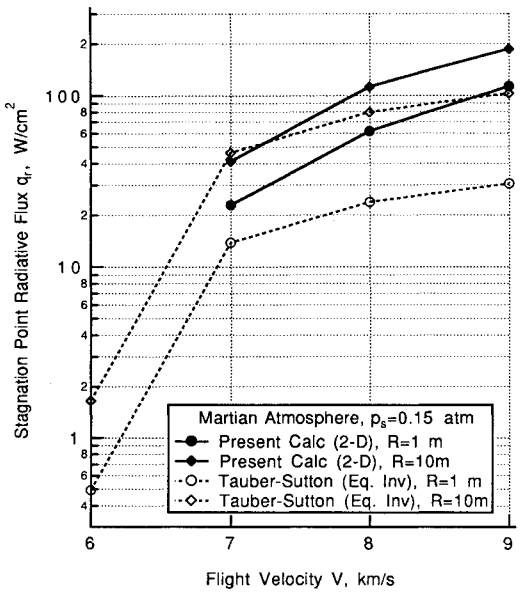

Fig. 17 Comparison between the stagnation point radiative heat fluxes predicted by the present models in the Martian atmosphere and those by the equilibrium-inviscid model of Tauber and Sutton,[59] for p_s = 0.15 atm and R = 1 and 10 m.

in the boundary layer. At higher velocities, presumably the nonequilibrium overshoot phenomenon is stronger than absorption. Between the R-values of 1–10 m, the present values approximately follow $q_r \propto R^{0.3}$.

One notes here that the present calculation ignores radiative cooling of the shock layer, while the work of Hartung et al. accounts for it. The extent of radiative cooling depends on the ratio between q_r and the energy flux $0.5\rho_\infty V^3$. For V = 9 km/s and R = 10 m, this ratio for the present calculation is nearly 3%. Under such an environment, ordinarily radiative cooling will substantially lower the temperature of the shock layer and consequently q_r. However, cooling is a cumulative phenomenon, i.e., reduction in temperature occurs progressively downstream. The nonequilibrium region immediately behind the shock wave is relatively unaffected by the cooling phenomenon.[60,61] Since the strongest contribution to radiative flux comes from this nonequilibrium region, the radiative cooling phenomenon is probably not as pronounced in the nonequilibrium case as in the equilibrium case. It goes without saying that, for a more precise calculation, both the nonequilibrium effect and the cooling effect must be accounted for.

According to the present calculation, q_r is about 19 W/cm^2 at V = 7 km/s and R = 1 m. At V = 9 km/s and R = 10 m, it is nearly 190 W/cm^2. Considering the fact that the convective heat transfer rates for a body of 1–10 m radius at p_s of 0.15 atm will be of the order of a few tens of W/cm^2 in this range of velocity and freestream density, one can conclude that radiative heating will have to be considered for flight velocities of 7 km/s or higher. Thermochemical nonequilibrium must be accounted for for accurate prediction of radiative heating rates.

Discussion

The analysis in the first part of this work, namely, the part concerning the thermochemical model, shows that vibrational temperature approaches the translational temperature relatively quickly. As mentioned earlier, this is caused by the relatively fast relaxation of the vibrational modes of the CO_2 molecules. This point agrees with the finding of previous investigators.[13–17] During the process of vibrational excitation, the CO_2 molecules are dissociated. The rate of dissociation of CO_2 is quite fast also. The ensuing chemical reactions break down CO molecules into C and O. However, equilibration of this process is slow first because the dissociation energy of CO is very high, and second because it is indirectly affected by the ionization processes which are slow. Because the species C has a relatively low ionization potential, its ionization can occur at relatively low temperatures. Most of the chemical processes can be considered to occur in a one-temperature environment where T and T_v are equal.

The present thermochemical model includes the species NCO. As Fig. 9b shows, concentration of NCO is substantial only immediately behind the shock wave where CO_2 is present. The species NCO enhances the rate of dissociation of CO_2 there. The concentration of NCO remains very small thereafter. Since dissociation of CO_2 is intrinsically very fast, neglecting the presence of NCO will not alter the overall rate of equilibration. Thus, one could legitimately remove NCO from the reaction scheme.

The molecular ions NO^+ and CO^+ attain a relatively high value immediately behind the shock wave. These species are important in that they provide the initial free electrons which are needed in triggering the electron impact ionization processes. The electron impact ionization processes are important in turn because they dictate the ultimate equilibration. Therefore, even though the concentrations are small, these molecular ions should be kept in the reaction scheme. On the other hand, the peak concentration of the O_2^+ species is considerably smaller than those of NO^+ and CO^+. Therefore, O_2^+ could be eliminated from the reaction scheme. This leaves the following 16 species to be considered for the study of Martian entries: Ar, C, N, O, C_2, N_2, O_2, CN, CO, NO, CO_2, C^+, O^+, CO^+, NO^+, and e^-. This reduction in the number of species will bring a corresponding simplification to the reaction scheme.

The second part of the present work, namely, the part that analyzes the radiative heating phenomenon, shows that strong radiation emanates in the nonequilibrium region immediately behind the shock wave. The nonequilibrium radiative heating rate is substantially larger than the corresponding rate for an equilibrium shock layer. This point agrees also with the conclusions of some of the earlier investigators.[15,16] This trend is qualitatively the same as in air.[6]

Though not presented here, calculations have been repeated by the present authors using a one-temperature model. The results confirmed that most chemical equilibration processes in a Martian gas mixture indeed proceed under a one-temperature environment. Radiative flux values for the blunt body are seen to be higher than those of the two-temperature calculations by about 20%.

Finally, accuracy of the parameters derived in the present work needs to be examined. The first part of the work shows that the rate parameters cannot be determined with a high accuracy, even though the selected values are consistent with the existing experimental data. Experimental verification should be made of the thermochemical behavior of the Martian-atmospheric gas mixture.

Conclusions

1) The nonequilibrium thermochemical model for the CO_2-N_2 mixtures developed in the present work leads to radiation predictions that are consistent with the existing experimental data to a flight velocity of up to about 9 km/s.

2) Approach of vibrational temperature toward translational temperature and dissociation of CO_2 are both fast behind a shock wave, but chemical equilibration is very slow because of slow CO dissociation and ionization.

3) At the postshock pressure of 0.15 atm, equilibration of thermochemical processes requires a distance of 9–27 cm for flight velocities between 6–9 km/s. The equilibration distances are substantially longer than in air.

4) In a shock layer over a blunt body, strong radiation emanates from the narrow nonequilibrium region behind the shock wave.

5) For a blunt body of nose radius between 1–10 m entering the Martian atmosphere at a velocity between 7–9 km/s, with a shock layer pressure of 0.15 atm, the radiative heat flux reaching the stagnation point wall is between 19–190 W/cm^2. Radiative heat flux varies with R approximately as $R^{0.3}$ at that pressure.

6) The thermochemical model calculation developed in the present work is subject to a substantial uncertainty. In order to reduce uncertainty, further work is necessary in both experimentation and computation.

Acknowledgments

The authors wish to express sincere thanks to E. E. Whiting for adapting and improving the computer code NONEQ for application to the Martian atmosphere, and to M. E. Tauber for valuable critiquing and suggestions.

References

[1]Braun, R. D., Powell, R. W., and Hartung, L. C., "Effect of Interplanetary Trajectory Options on a Manned Mars Aerobrake Configuration," NASA TP 3019, Aug. 1990.

[2]Gamble, J. D., "JSC Pre-Phase A Study Mars Rover Sample Return Mission Aerocapture, Entry, and Landing Element," Lyndon B. Johnson Space Center, JSC-23230, Houston, TX, May 1989.

[3]Tauber, M. E., Bowles, J. V., and Yang, L., "The Use of Atmospheric Braking During Mars Mission," AIAA Paper 89-1730, June 1989.

[4]Seiff, A., and Kirk, D. B., "Structure of the Atmosphere of Mars in Summer at Mid-Latitudes," *Journal of Geophysical Research*, Vol. 82, No. 28, 1977, pp. 4364–4378.

[5]Woodward, H. T., "Predictions of Shock Layer Radiation from Molecular Band Systems in Proposed Planetary Atmospheres," NASA TN D-3850, Feb. 1967.

[6]Park, C., "Assessment of Two-Temperature Kinetic Model for Ionizing Air," *Journal of Thermophysics and Heat Transfer*, Vol. 3, No. 3, 1989, pp. 233–244.

[7]Millikan, R. C., and White, D. R., "Systematics of Vibrational Relaxation," *Journal of Chemical Physics*, Vol. 39, No. 12, 1963, pp. 3209–3213.

[8]Camac, M., "CO_2 Relaxation Processes in Shock Waves," *Fundamental Phenomena in Hypersonic Flow*, edited by J. G. Hall, Cornell Univ. Press, Ithaca, NY, 1966, pp. 195–215.

[9]Baulch, D. L., Drysdale, D. D., Duxbury, J., and Grant, S. J., "Evaluated Kinetic Data for High Temperature Reactions, Vol. 3: Homogeneous Gas Phase Reactions of the O_2-O_3 System, the CO-O_2-H_2 System, and of Sulphur-Containing Species," Butterworths, London, 1987.

[10]Baulch, D. L., Duxbury, J., Grant, S. J., and Montague, D. C., "Evaluated Kinetic Data for High Temperature Reactions. Vol. 4, Homogeneous Gas Phase Reactions of Halogen- and Cyanide-Containing Species," *Journal of Physical and Chemical Reference Data*, Vol. 10, Supplement 1, 1981.

[11]Hindelang, F. J., "Coupled Vibration and Dissociation Relaxation Behind Strong Shock Waves in Carbon Dioxide," NASA TR R-253, Feb. 1967.

[12]Hahne, G. E., "Vibrational Relaxation in Carbon Monoxide Gas," Hochschule der Bundeswehr München, Fachbereich Luft- und Raumfahrttechnik, Wissenschaftliche Einrichtung Strömungsmechanik, Rept. 1/80, 1980.

[13]Howe, J. T., Viegas, J. R., and Sheaffer, Y. S., "Study of the Nonequilibrium Flow Field Behind Normal Shock Waves in Carbon Dioxide," NASA TN D-1885, June 1963.

[14]Howe, J. T., and Sheaffer, Y. S., "Chemical Relaxation Behind Strong Normal Shock Waves in Carbon Dioxide Including Interdependent Dissociation and Ionization Processes," NASA TN D-2131, Feb. 1964.

[15]McKenzie, R. L., "The Qualitative Behavior of Effects of Nonequilibrium Chemistry Behind Strong Shock Waves in Gas Mixtures of CO_2 and N_2," *Proceedings of the AIAA/AAS Stepping Stones to Mars Meeting* (Baltimore, MD), AIAA, New York, March 1966, pp. 391–409.

[16]Freeman, G. N., and Oliver, C. C., "Chemical Nonequilibrium Viscous Radiating Blunt Body Shock Layers in CO_2-N_2 Atmospheres," AIAA Paper 71-35, Jan. 1971.

[17]Candler, G. V., "Computation of Thermochemical Nonequilibrium Martian Atmospheric Entry Flows," AIAA Paper 90-1695, June 1990.

[18]Arnold, J. O., Reis, V. H., and Woodward, H. T., "Theoretical and Experimental Studies of Equilibrium and Nonequilibrium Radiation to Bodies Entering Postulated Martian and Venusian Atmospheres at High Speeds," AIAA Paper 65-0166, Jan. 1965.

[19]Thomas, G. M., and Menard, W. A., "Experimental Measurements of Nonequilibrium and Equilibrium Radiation from Planetary Atmospheres," *AIAA Journal*, Vol. 4, No. 2, 1966, pp. 227–237.

[20]Nealy, J. E., and Haggard, K. V., "A Shock Tube Study of Radiation Behind Shock Waves in CO_2 with Application to Venus Entry," *Recent Developments in Shock Tube Research: Proceedings of the 9th International Symposium on Shock Tubes and Waves*, edited by D. Bershader and W. Griffith, Stanford Univ. Press, Stanford, CA, 1973, pp. 330–339.

[21]Nealy, J. E., "An Experimental Study of Ultraviolet Radiation Behind Incident Normal Shock Waves in CO_2 at Venusian Entry Speeds," AIAA Paper 75-1150, Sept. 1975.

[22]Arnold, J. O., and Nicholls, R. W., "A Shock-Tube Determination of the CN Ground State Dissociation Energy and Electronic Transition Moments for the CN Violet and Red Band Systems," *Recent Developments in Shock Tube Research: Proceedings of the 9th International Symposium on Shock Tubes and Waves*, edited by D. Bershader and W. Griffith, Stanford Univ. Press, Stanford, CA, 1973, pp. 340–351.

[23]Dunn, M. G., "Measurement of $C^+ + e^- + e^-$ and $CO^+ + e^-$ Recombination in Carbon Monoxide Flows," *AIAA Journal*, Vol. 9, No. 11, 1971, pp. 2184–2191.

[24]Davies, W. O., "Carbon Dioxide Dissociation at 6000 to 11,000 K," *Journal of Chemical Physics*, Vol. 43, No. 8, 1965, pp. 2809–2815.

[25]Burmeister, M., and Roth, P., "ARAS Measurements on the Thermal Decomposition of CO_2 Behind Shock Waves," *AIAA Journal*, Vol. 28, No. 3, 1990, pp. 402–405.

[26]Appleton, J. P., Steinberg, M., and Liquornik, D. J., "Shock-Tube Study of Carbon Monoxide Dissociation Using Vacuum-Ultraviolet Absorption," *Journal of Chemical Physics*, Vol. 52, No. 5, 1970, pp. 2205–2221.

[27]Hanson, R. K., "Shock-Tube Study of Carbon Monoxide Dissociation Kinetics," *Journal of Chemical Physics*, Vol. 60, No. 12, 1974, pp. 4970–4976.

[28]Mick, H. J., and Roth, P., "High Temperature Thermal Decomposition of CO and CN," 18th International Symposium on Shock Waves and Tubes, Sendai, Japan, 1991.

[29]Lindackers, D., Burmeister, M., and Roth, P., "High-Temperature Kinetics of the Reaction CN + CO_2," *Combustion and Flame*, Vol. 81, Nos. 3 and 4, 1990, pp. 251–259.

[30]Thorne, L. R., Branch, M. C., Chandler, D. W., Kee, R. J., and Miller, J. A., "Hydrocarbon/Nitric Oxide Interactions in Low-Pressure Flames," *Proceedings of the 21st Symposium (International) on Combustion*, The Combustion Inst., Pittsburgh, PA, 1986, p. 965.

[31]Colket, M. B., III, "Cyanogen Pyrolisis and the CN + NO Reaction Behind Incident Shock Waves," *International Journal of Chemical Kinetics*, Vol. 16, No. 4, 1984, pp. 353–369.

[32]Mulvihill, J. N., and Phillips, L. F., "Breakdown of Cyanogen in Fuel-Rich $H_2/N_2/O_2$ Flames," *Proceedings of the 15th Symposium (International) on Combustion*, The Combustion Inst., Pittsburgh, PA, 1975, pp. 1113–1122.

[33]Natarajan, K., and Roth, P., "A Shock Tube Study of CN Radical Reactions with H_2 and NO Verified by H, N and O Atom Measurements," *Proceedings of the 21st Symposium (International) on Combustion*, The Combustion Inst., Pittsburgh, PA, 1986, p. 729.

[34]Mozzhukhin, E., Burmeister, M., and Roth, P., "High Temperature Dissociation of Cyanogen Radical," *Berichte Bunsengesellschaft der Physikalischen Chemie*, Vol. 93, No. 1, 1989, pp. 70–75.

[35]Lifshitz, A., and Frenklach, M., "Oxidation of Cyanogen. II. The Mechanism of the Oxidation," *International Journal of Chemical Kinetics*, Vol. 12, No. 3, 1980, pp. 159–168.

[36]Louge, M. Y., and Hanson, R. K., "Shock Tube Study of Cyanogen Oxidation Kinetics," *International Journal of Chemical Kinetics*, Vol. 16, No. 3, 1984, pp. 231–250.

[37]Schacke, H., Schmatjko, K. J., and Wolfrum, J., "Reactions of Molecules in Defined Vibrational States. I. Reactions of CN(v) with Atomic and Molecular Oxygen," *Berichte Bunsengesellschaft für Physikalischen Chemie*, Vol. 77, No. 4, 1973, pp. 248–253.

[38]Beck, W. H., and Mackie, J. C., "Formation and Dissociation of C_2 from High Temperature Pyrolysis of Acetylene," *Journal of the Chemical Society: Faraday Transactions I*, Vol. 71, No. 6, 1975, pp. 1363–1371.

[39]Thielen, K., and Roth, P., "Shock Wave Studies on the Initiation of Reaction CO + O_2," *Berichte Bunsengesellschaft für Physikalische Chemie*, Vol. 87, No. 10, 1983, pp. 920–925.

[40]Schmatjko, K. J., and Wolfrum, J., "Direct Measurement of the Product Energy Distribution in the Reaction of O-Atoms with CN Radicals," *Proceedings of the 16th Symposium (International) on Combustion*, The Combustion Inst., Pittsburgh, PA, 1977, pp. 819–827.

[41]Slack, M. W., "Kinetics and Thermodynamics of the CN Molecule. 3. Shock Tube Measurements of CN Dissociation Rates," *Journal of Chemical Physics*, Vol. 64, No. 1, 1976, pp. 228–236.

[42]Atkinson, R., Baulch, D., Cox, R. A., Hampson, R. F., Jr., Kerr, J. A., and Troe, J., "Evaluated Kinetic and Photochemical Data for Atmospheric Chemistry: Supplement III," *International Journal of Chemical Kinetics*, Vol. 21, No. 2, 1989, pp. 115–1150.

[43]Park, C. S., "Studies of Radiation Emission from the Simulated Shock Layer of the Huygens Probe," Ph.D. Dissertation, Dept. of Aeronautics and Astronautics, Stanford Univ., Stanford, CA, 1991.

[44]Park, C., "Review of Chemical-Kinetic Problems of Future NASA Missions, I: Earth Entries," *Journal of Thermophysics and Heat Transfer*, Vol. 7, No. 3, 1993, pp. 385–398.

[45]Park, C., "Problems of Rate Chemistry in the Flight Regimes of Aeroassisted Orbital Transfer Vehicles," *Thermal Design of Aeroassisted Orbital Transfer Vehicles*, edited by H. F. Nelson, Vol. 96, Progress in Astronautics and Aeronautics, AIAA, New York, 1985, pp. 511–537.

[46]Park, C. "Calculation of Nonequilibrium Radiation in the Flight Regimes of Aeroassisted Orbital Transfer Vehicles," *Thermal Design of Aeroassisted Orbital Transfer Vehicles*, edited by H. F. Nelson, Vol. 96, Progress in Astronautics and Aeronautics, AIAA, New York, 1985, pp. 395–418.

[47]Park, C., "Assessment of Two-Temperature Kinetic Model for Dissociating and Weakly-Ionizing Nitrogen," *Journal of Thermophysics and Heat Transfer*, Vol. 2, No. 1, 1988, pp. 8–16.

[48]Park, C., *Nonequilibrium Hypersonic Aerothermodynamics*, Wiley, New York, 1990.

[49]Whiting, E. E., and Park, C., "Radiative Heating at the Stagnation Point of the Aeroassist Flight Experiment Vehicle," NASA TM 102829, Nov. 1990.

[50]Hornung, H. G., "Induction Time for Nitrogen Dissociation," *Journal of Chemical Physics*, Vol. 56, No. 6, 1972, pp. 3172, 3173.

[51]Eckstrom, D. J., "Vibrational Relaxation of Shock-Heated N_2 by Atomic Oxygen Using the IR Tracer Method," *Journal of Chemical Physics*, Vol. 59, No. 6, 1973, pp. 2787–2795.

[52]Kiefer, J. H., and Lutz, R. W., "The Effect of Oxygen Atoms on the Vibrational Relaxation of Oxygen," *Proceedings of the 11th Symposium (International) on Combustion*, The Combustion Inst., Pittsburgh, PA, 1967, pp. 67–76.

[53]Center, R. E., "Vibrational Relaxation of Carbon Monoxide and Carbon Dioxide by Atomic Oxygen," *Recent Developments in Shock Tube Research: Proceedings of the 9th International Symposium on Shock Tubes and Waves*, edited by D. Bershader and W. Griffith, Stanford Univ. Press, Stanford, CA, 1973, pp. 383–394.

[54]Griem, H. R., *Plasma Spectroscopy*, McGraw-Hill, New York, 1964.

[55]Park, C., "A Review of Reaction Rates in High Temperature Air," AIAA Paper 89-1740, June 1989.

[56]Park, C., and Davies, C. B., "Aerothermodynamics of Sprint-Type Manned Mars Missions," *Journal of Spacecraft and Rockets*, Vol. 27, No. 6, 1990, pp. 589–596.

[57]Page, W. A., Compton, D. L., Borucki, W. J., Ciffone, D. L., and Cooper, D. M., "Radiative Transport in Inviscid Nonadiabatic Stagnation-Region Shock Layers," *Thermal Design Principles of Spacecraft and Entry Bodies*, edited by J. T. Bevans, Vol. 21, Progress in Astronautics and Aeronautics, AIAA, New York, 1969, pp. 75–114.

[58]Hartung, L. C., Sutton, K., and Brauns, F., "Equilibrium Radiative Heating Tables for Aerobraking in the Martian Atmosphere," NASA TM 102659, May 1990.

[59]Tauber, M. E., and Sutton, K., "Stagnation Point Radiative Heating Relations for Earth and Mars Entries," *Journal of Spacecraft and Rockets*, Vol. 28, No. 1, 1991, pp. 40–42.

[60]Hartung, L. C., Mitcheltree, R. A., and Gnoffo, P. A., "Coupled Radiation Effects in Thermochemical Nonequilibrium Shock Capturing Flowfield Calculations," AIAA Paper 92-2868, July 1992.

[61]Gokcen, T., "Computation of Nonequilibrium Radiating Shock Layers," AIAA Paper 93-0144, Jan. 1993.